RESEARCH ARTICLE

Phosphoproteome analysis of an early onset mouse model (TgCRND8) of Alzheimer's disease reveals temporal changes in neuronal and glia signaling pathways

Fangjun Wang[1,2], Alexandre P. Blanchard[2,3]*, Fred Elisma[2], Matthew Granger[2,3], Hongbin Xu[2,3], Steffany A. L. Bennett[2,3]**, Daniel Figeys[2] and Hanfa Zou[1]***

[1] Key Lab of Separation Sciences for Analytical Chemistry, National Chromatographic R & A Center, Dalian Institute of Chemical Physics, Chinese Academy of Sciences, Dalian, P. R. China
[2] Ottawa Institute of Systems Biology, University of Ottawa, Ottawa, Canada
[3] Neural Regeneration Laboratory, Department of Biochemistry, Microbiology, and Immunology University of Ottawa, Ottawa, Canada

Received: September 8, 2012
Revised: October 19, 2012
Accepted: November 8, 2012

Sustained exposure to soluble amyloid β ($A\beta_{42}$) oligomers is predicted to impair synaptic function in the hippocampal-entorhinal circuit, signaling synaptic loss and precipitating cognitive impairment in Alzheimer's disease. Regional changes in overall patterns of protein phosphorylation are likely crucial to promote transition from a presymptomatic to a symptomatic state in response to accumulating $A\beta_{42}$. Here, we used unbiased proteomic approaches to compare the phosphoproteome of presymptomatic and symptomatic TgCRND8 mice and identify network disruptions in signaling pathways implicated in the manifestation of behavioral indices of learning and memory impairment. Phosphopeptide enrichment with triple isotopic dimethylation labeling combined with online multidimensional separation and MS was used to profile phosphoproteome changes in 2- and 6-month-old TgCRND8 mice and congenic littermate controls. We identified 1026 phosphopeptides representing 1168 phosphorylation sites from 476 unique proteins. Of these, 595 phosphopeptides from 293 unique proteins were reliably quantified and 139 phosphopeptides were found to change significantly in the hippocampus of TgCRND8 mice following conversion from a presymptomatic to a symptomatic state.

Keywords:
Alzheimer's disease / Animal model / Animal proteomics / MS / Phosphoproteomics / TgCRND8

Additional supporting information may be found in the online version of this article at the publisher's web-site

1 Introduction

Two central pathological events define Alzheimer's disease (AD): (i) the intraneuronal accumulation of neurofibrillary tangles composed of hyperphosphorylated tau, and (ii) the aberrant processing of the amyloid precursor protein (APP)

Correspondence: Dr. Daniel Figeys, University of Ottawa – BMI, 451 Smyth Road Ottawa K1H 8M5, Canada
E-mail: dfigeys@uottawa.ca
Fax: 613-562-5655

Abbreviations: Aβ, amyloid β; **AD**, Alzheimer's disease; **APP**, amyloid precursor protein; **CDK5**, cyclin-dependent kinase 5; **DLGAP**, Discs, large homolog-associated protein; **DPYSL**, dihydropyrimidinase-related protein; **FDR**, false-discovery rate; **GSK3β**, glycogen synthase kinase-3 beta; **H**, heavy; **L**, light; **M**, medium; **MAP1a**, microtubule-associated protein 1A; **MAP1b**, microtubule-associated protein 1B; **MAP2**, microtubule-associated protein 2; **MBP**, myelin basic protein; **NonTg**, non transgenic; **SHANK3**, SH3 and multiple ankyrin repeat domains protein 3; **Tg**, Transgenic

*These authors contributed equally to this work.
**Additional corresponding authors: Dr. S. Bennett, E-mail: sbennet@uottawa.ca; Dr. Hanfa Zou, E-mail: hanfazou@dicp.ac.cn.
Colour Online: See the article online to view Figs. 1, 3 and 4 in colour.

to different toxic assemblies of amyloid β (Aβ) peptides [1]. The most damaging of these peptide assemblies are soluble oligomeric $A\beta_{42}$ [2]. Genomic evidence confirms that mutations in either the APP gene or the presenilin genes accelerate $A\beta_{42}$ biosynthesis resulting in the early onset familial AD [2]. Sustained exposure to soluble $A\beta_{42}$ oligomers is predicted to impair synaptic function in the hippocampal-entorhinal circuit, signaling synaptic loss, and precipitating cognitive impairment [2–5]. Despite these strong proofs that $A\beta_{42}$ accumulation is a driving pathology in AD, underlying disruptions in signal transduction pathways have only begun to be elucidated.

Regional changes in overall patterns of protein phosphorylation are likely crucial to promote transition from a presymptomatic to a symptomatic state in response to accumulating $A\beta_{42.}$ These changes would contribute to disruption of multiple signaling pathways and, in part, contribute to the "change in state" postulated to be necessary for cognitive decline [6]. The hyperphosphorylation of tau represents a primary example of "phospho-pathology" wherein progressive alterations in phosphorylation status alter the capacity of tau to stabilize microtubules thereby impairing axonal transport [7]. Certainly, the severity of AD dementia is highly correlated with the degree of abnormal tau phospho-processing in the hippocampal-entorhinal circuit associated with progressive aggregation and deposition of neurofibrillary tangles [8]. Significant alterations in phosphoproteome status have already been reported in postmortem hippocampus of AD patients relative to age-matched controls [9]. It is not known whether these changes are a late-stage event manifested following catastrophic memory failure and neuronal loss, or whether key phospho-signaling pathways are disrupted upon transition from a presymptomatic to symptomatic disease state in response to accumulating $A\beta_{42}$.

To address this question, we applied unbiased phosphoproteomic approaches to study a rapid onset mouse model of AD and identify network disruptions in phosphorylation-dependent signaling pathways exhibited upon transition from a presymptomatic to a symptomatic state. The TgCRND8 (Tg) mouse model expresses the human APP 695 gene with both familial Swedish and Indiana AD mutations under the control of the prion protein promoter [10–12]. This model is widely used for large-scale "omics studies" of AD associated with $A\beta_{42}$ biogenesis [11, 13–15]. Here, we show that the TgCRND8 hippocampal phosphoproteome is significantly altered between 2 and 6 months of age. Briefly, we applied phosphopeptide enrichment with triple isotopic dimethylation labeling combined with online multidimensional separation and MS-to-profile phosphoproteome changes in hippocampi of a presymptomatic (2-month-old) and a symptomatic (6-month-old) Tg mice relative to NonTg littermates. A total of 1026 phosphopeptides, representing 1168 phosphorylation sites from 476 unique proteins was identified. Of these, 595 phosphopeptides from 293 unique proteins were quantified and 139 phosphopeptides were found to change significantly in the hippocampi of TgCRND8 mice compared to controls between 2 and 6 months of age. Network alterations in identified phospho-signaling pathways within the hippocampus are discussed with respect to TgCNRD8 transition from a presymptomatic to a symptomatic state.

2 Material and methods

2.1 Animals and tissues

TgCRND8 mice on a mixed C57BL/6 X C3H hybrid background were kindly provided by Dr. Fraser (University of Toronto) and were backcrossed for five generations (N5) to a C57BL/6 lineage in the Bennett laboratory. C57BL/6Crl were mice obtained from Charles Rivers Laboratories (Senneville, Canada). Heterozygote Tgs and congenic wild-type (NonTg) littermates were maintained by breeding NonTg females with Tg males. The TgCRND8 line expresses a double mutant form (KM670/671NL+V717F) of the human APP gene under the control of the prion protein promoter [10]. Previous studies have shown that pathogenic increases in the ratio of $A\beta_{42}/A\beta_{40}$ in a mixed C57BL/6 X C3H hybrid background are first detected at 2.5 months of age and behavioral learning and memory impairment detected between 3 and 4 months of age [10]. Here, a total of 62 female N5 Tg ($n = 26$) and wild-type (NonTg, $n = 36$) littermates was analyzed. For genotyping, genomic DNA was isolated from biopsied tail and PCR amplification was 3 min at 94°C followed by 35 cycles of 20 s at 94°C, 20 s at 68°C, and 90 s at 72°C terminating after the last cycle with 7 min at 73°C. Primers were as follows: 5′-GGC CGC GGA GAA ATG AAG AAA CGC CAA GCG CCG TGA CT-3′ (forward) and 5′- TGT CCA AGA TGC AGC AGA ACG GCT ACG AAA A-3′ (reverse). Tg mice produce a 1 kB amplicon. To verify template integrity, all animals were genotyped for the platelet-activating factor receptor. PCR amplification was 10 min at 95°C followed by 30 cycles of 20 s at 94°C, 20 s at 65°C, and 50 s at 70°C. Primers were as follows 5′-TAT GGC TGA CCT GCT CTT CCT GAT-3′ (forward) and 5′- TAT TGG GCA CTA GGT TGG TGG AGT-3′ (reverse). Tg and NonTg mice produce a 289-kB amplicon. Behavioral assessments were performed on $n = 5$ Tg and $n = 12$ NonTg mice at 2 months of age and on $n = 5$ Tg and $n = 8$ NonTg mice at 6 months of age. An additional $n = 3$ mice per genotype and time point were used to quantify Aβ plaque load. For Western analyses, $n = 2$ mice/genotype were analyzed at 2, 4, and 6 months of age. For proteomic assessments, the hippocampi (including dorsal and ventral regions) of two females per genotype and time point were dissected, immediately flash-frozen in liquid nitrogen, and stored at −80°C until protein extraction. All animal manipulations were performed in strict accordance with the ethical guidelines for experimentation established by the Canadian Council for Animal Care and with the approval of the University of Ottawa Animal Care Committee for the ethical treatment of experimental animals.

2.2 Behavioral assessment

Learning and memory was assessed in the Morris Water Maze (Noldus Information Technology). The apparatus consisted of a blue plastic pool measuring 134.5 cm in diameter and 53.3 cm deep with floor insert. The pool was filled with water rendered opaque with white water-soluble nontoxic paint to a depth of 1 cm above the 10 cm diameter white escape platform located in the back-right quadrant. Water temperature was maintained at 21°C. Visual cues consisted of a square and an "X" located within visual range of the swimming mice at front (opposite entry) and left walls of the test room (2.98 m × 3.97 m × 2.62 m), respectively. Mice were habituated to the room 1 h prior to testing. The room was lit with overhead white light of 100 lux. Constant white noise at 70 dB was provided during acclimatization and testing. Each mouse completed four trials per day. Each trial lasted until the animal found the platform or for a maximum of 60 s. Mice that failed to find the platform within this time period were guided to the platform by the experimenter and then removed from the pool. Each trial was randomized to one of four possible starting locations. Mice were run in cohorts of 6–12 with 20 min in between in each trial. Performance was recorded with a video camera mounted directly above the pool and data acquired and analyzed with Ethovision v7 software. Data were analyzed by repeated measures (test day) two-way ANOVA (test day and genotype) as indicated followed by Holm–Sidak's multiple comparisons test maintaining family-wise error at either 0.05 or 0.01. Analyses were performed using Prism 6.0a (GraphPad).

2.3 Aβ plaque quantitation

Plaque number was determined as described previously [16]. Animals were euthanized by lethal injection of sodium pentobarbital and transcardially perfused with 10 mM PBS (10 mM sodium phosphate and 154 mM NaCl) followed by 3.7% paraformaldehyde in 10 mM PBS. Brains were removed and postfixed for 24 h in this same solution. Brains were switched to 10 mM PBS, paraffin-embedded, and serially sectioned by the uOttawa Pathology Core Facility. Every tenth section in a series of sagittal 10 μm serial sections through one paraffin-embedded hemisphere from start of hippocampus to midline was analyzed. Deparaffinized, hydrated sections were incubated in 10% formic acid, pH 1.6–2.0 for 10 min, washed repeatedly in PBS, and incubated overnight with mouse anti-4G8 (Covance SIG-39220 mouse at 1:500) in Ab buffer (3% BSA, 0.3% Triton X-100 in 10 mM PBS). 4G8 recognizes both murine and human Aβ. Secondary antibody was biotin-labeled goat antimouse IgG (1:300, Sigma B9904) detected with extravidin-horseradish peroxidase (1:20 Sigma, E2886) using 3,3′-diaminobenzidine tetrahydrochloride tablets as substrate (Sigma D5905). Images were captured on a Leica DMXAR2 microscope and converted to binary images for quantification of plaque number and hippocampal area using the OpenLab v5.08 Advanced Measurements module. Plaques were defined as immunoreactive, compacted, and spherical aggregates greater than 10 μm in diameter. Data were expressed as mean ± SEM per section and were analyzed two-way ANOVA (age and genotype) by two-way ANOVA followed by Holm–Sidak's multiple comparisons test maintaining family-wise error at either 0.05 or 0.01. Analyses were performed using Prism 6.0a (GraphPad).

2.4 Immunoblotting

Total proteins were extracted from a whole mouse hippocampus homogenized in RadioImmunoprecipitation Assay (RIPA) buffer (1% Nonidet P40 substitute, 0.5% sodium deoxycholate, 0.1% sodium dodecyl sulfate, 1 mM sodium fluoride, 1 mM sodium orthovanadate, 300 μg/mL aprotinin, and 100 μg/mL phenylmethylsulfonyl fluoride in 10 mM phosphate-buffered saline [10 mM phosphate, 154 mM NaCl]) using a Tissue-Tearor (Biospec Products). The protein concentration was determined using the Bio-Rad DC protein assay kit (Bio-Rad 500–0112) in accordance with the manufacturer's guidelines. Protein samples of 15 μg were incubated for 10 min at 70°C in NuPAGE lithium dodecyl sufate (LDS) sample buffer and resolved on an NuPAGE 4–12% SDS–PAGE gel (Invitrogen). Proteins were transferred onto a nitrocellulose membrane (Pall Life Sciences 66485) and blocked for 30 min in 5% non-fat milk in TBS-T (50 mM Tris base, 150 mM NaCl, 0.1% Tween 20). Western blot analysis was performed by an overnight probe at 4°C with α-myelin basic protein (MBP) (Sigma M3821 rabbit at 1:4000), α-APP (4G8 Covance SIG-39220 mouse at 1:1000), or α-actin (Cederlane CLT9001 mouse at 1:15 000). Secondary antibody, horseradish peroxidase-conjugated α-mouse (Rockland; 610–1319-0500 at 1:10 000) or α-rabbit (GE Healthcare; NA934V at 1:10 000), were incubated for 1 h at room temperature. The signals were revealed by chemiluminescence using Immobilon Western (Millipore WBKLS0500) and the protein expression was quantified by ImageJ analysis software (v1.45 National Institutes of Health (NIH)) based on densitometry.

2.4.1 Protein extraction and sample preparation for MS

A schematic of the processing of Tg and NonTg hippocampi for labeling and enrichment of phosphopeptides is presented in Fig. 1A. The hippocampal formation from one cerebral hemisphere per animal was finely minced, and incubated in 200 μL extraction buffer (8 M Urea, 50 mM Tris pH 8.2, 65 mM DTT, EDTA-free protease inhibitor, and phosphatase inhibitor cocktail tablets (Roche)). The tissue was sonicated at 24 W for 20 s with 30 s intermission on ice. Following a

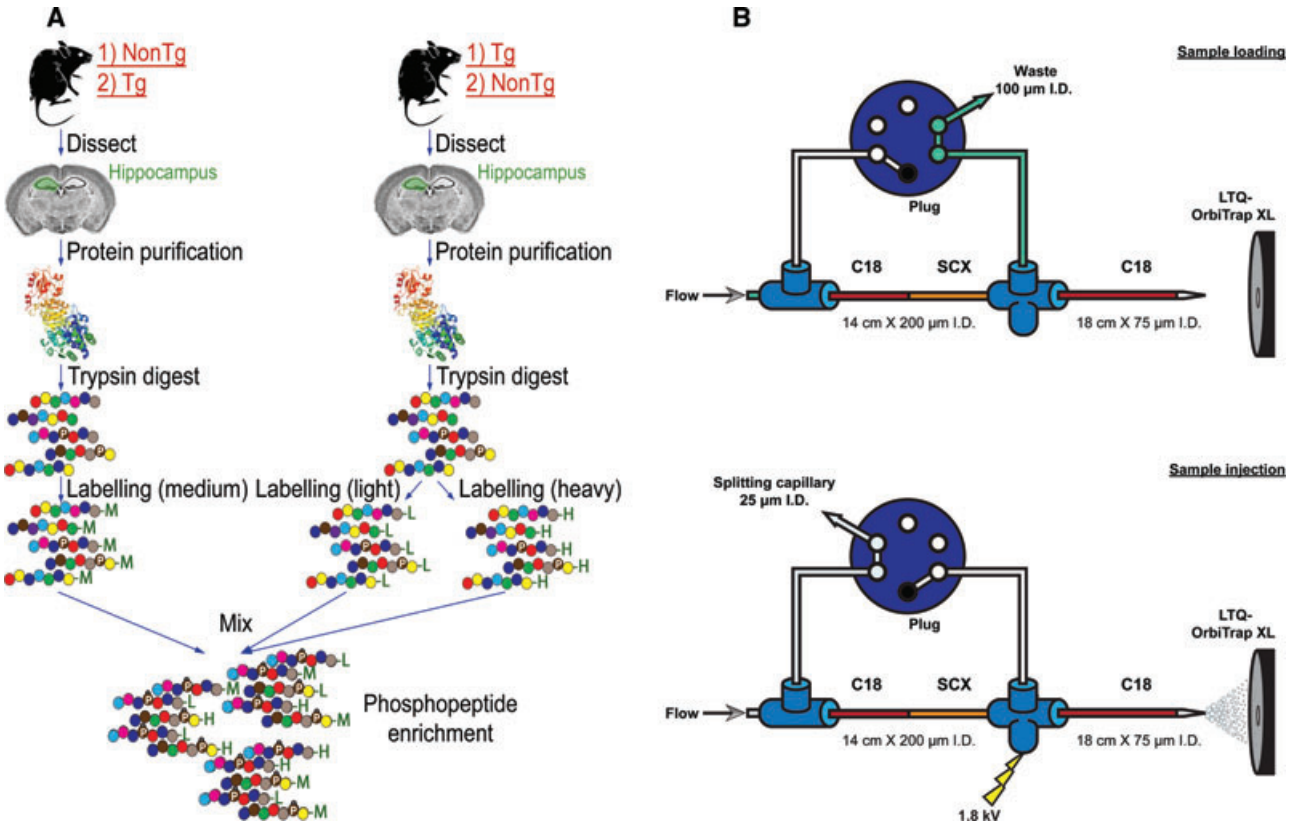

Figure 1. (A) Schematic of the processing of the tansgenic (Tg) and NonTg hippocampal samples for labeling and enrichment of phosphopeptides. (B) Schematic diagram of the vent sample injection system.

20 min incubation on ice and a centrifugation at 22 000 × *g* for 15 min, the supernatant was subjected to chloroform–methanol precipitation [17] and protein redissolved into 1 mL 8 M Urea, 50 mM Tris pH 8.2 buffer. The protein concentration was measured using the *DC* Protein Assay (Bio-Rad) as per manufacturer's protocol. The proteins were reduced using 5 mM DTT (Sigma) at 60°C for 1 h and alkylated with 10 mM iodoacetamide (Sigma) in the dark at room temperature for 40 min. The solution was diluted to 1 M urea by the addition of 50 mM Tris pH 8.2 buffer, digested overnight with 1:50 w/w sequence-grade trypsin (Promega), and the enzymatic reaction was stopped by the addition of 0.25%TFA. The peptidic solution was loaded onto a prewashed [(i) 1 mL ACN; (ii) 1 mL 0.1% formic acid aqueous solution], and pre-equilibrated (1 mL 50 mM sodium phosphate pH 7.5) 200 mg tC18 cartridge (Waters). To label proteins (Table 1), 5 mL isotopic labeling reagents containing (i) 0.2% CH_2O and 30 mM $NaBH_3CN$ (light [L] form labeling); or (ii) 0.2% CD_2O and 30 mM $NaBH_3CN$ (intermediate [M] form labeling); or (iii) 0.2% $^{13}CD_2O$ and 30 mM $NaBD_3CN$ (heavy [H] form labeling) were added (Table 1) [18]. After a wash with 1 mL 0.1% formic acid aqueous solution, the isotopic-labeled peptides were eluted from the tC18 cartridge using 1 mL 80% ACN. The eluted peptides were lyophilized to powder and stored at –80°C.

Table 1. The labeling reagents combination, labeling group, and mass shift for each isotopic labeling

Label	Light (L)	Intermediate (M)	Heavy (H)
Formaldehyde	CH_2O	CD_2O	$^{13}CD_2O$
Cyanoborohydride	$NaBH_3CN$	$NaBH_3CN$	$NaBD_3CN$
Labeling group	$2CH_3$	$2CHD_2$	$2^{13}CD_3$
Mass shift	+28.0313	+32.0564	+36.0757

2.4.2 Phosphopeptide enrichment

The procedures for preparation of the Ti^{4+}-IMAC monodisperse microspheres were as described previously [19]. The Ti^{4+}-IMAC microspheres were well dispersed into 80% ACN, 6% TFA aqueous solution at a concentration of 10 mg/mL. For comparative analyses, the same amount of isotopic dimethyl-labeled samples were dissolved into 0.1% formic acid aqueous solution and mixed. Then, the labeled peptides mixture was incubated with ten times Ti^{4+}-IMAC microspheres (w/w). Following 30 min of incubation at 4°C, the Ti^{4+}-IMAC microspheres with the adsorbed phosphopeptides were collected by centrifugation at 22 000 × *g* for 15 min. The microspheres were then successively washed with 500 μL of an aqueous solution of 50% ACN, 6% TFA, and 200 mM

NaCl, and then with 500 μL of an aqueous solution of 30% ACN and 0.1% TFA to remove nonspecific adsorption. Finally, 500 μL $NH_3 \cdot H_2O$ (12.5%) was used to elute the enriched phosphopeptides from the microspheres by stirring for 15 min at 4°C and sonicating for 15 min at 4°C. After centrifugation at 22 000 × *g* for 15 min, the phosphopeptide-containing supernatant was collected and lyophilized under vacuum at 45°C for 15 min.

2.4.3 Online multidimensional separation and nano-LC-MS/MS detection

A vent sample injection system was established for this study (Fig. 1B). A 14 cm × 200 μm id biphasic trap column with a 7-cm-long phosphate strong cation exchange monolith adjacent to a 7 cm-long C18 packing material (C18 AQ, 5 μm, 300 Å, Dr. Maisch GmbH, Ammerbuch, Germany) was used for sample injection. A 75 μm id tip column (New Objective Inc.) packed with an 18 cm-long C18 material (C18 AQ, 3 μm, 120 Å, Dr. Maisch GmbH) was used for peptides separation [20, 21]. The sample was injected into the trap column with a flow rate of 10 μL/min for 8 min, and the separation flow rate was adjusted to about 300 nL/min. After sample loading onto the biphasic trap column, the peptides were separated using a RP binary gradient and were detected by MS. 0.1% formic acid aqueous solution (solvent A) and 0.1% formic acid ACN (solvent B) were used as mobile phases for RP gradient separation. The RP binary gradient was set as follows: for the first 5 min, the mobile phase was ramped from 1 to 5% solvent B; for the next 140 min, the mobile phase was ramped from 5 to 30% solvent B, and finally for the next 5 min, the mobile phase was ramped from 30 to 90% solvent B and maintained at 90% solvent B for the next 8 min. The systems was re-equilibrated using 100% of solvent A for 12 min. Peptide fractions were transferred from the strong cation exchange monolith column to the separation column by NH_4AC (pH 2.7) salt step elutions. The NH_4AC (pH 2.7) salt steps were as follows: 5, 10, 15, 20, 25, 30, 35, 40, 45, 50, 55, 60, 80, 100, and 1000 mM. Each salt step lasted 8 min at a flow rate of 300 nL/min, and was followed by RP binary gradient separation and MS/MS detection.

MS detection was performed using an LTQ-OrbiTrap XL (Thermo, San Jose, CA, USA). The temperature of the ion-transfer capillary was 200°C, the electrospray voltage was +1.8 kV, and the normalized collision energy was 35%. One microscan was set for each MS and MS/MS scan. The MS full scans were acquired in centroid mode from m/z 400 to 2000 in the OrbiTrap with a resolution of 60 000, and the MS/MS scans were acquired in the LTQ linear ion-trap. All MS and MS/MS spectra were acquired in the data-dependent analysis mode, in which the ten most intense ions within an MS scan were selected for MS/MS scan by CID. The target ion setting was 5e5 and 3e4, with a maximum fill time of 500 and 100 ms, for the OrbiTrap and LTQ scans, respectively. The dynamic exclusion function was as follows: repeat count 2, repeat duration 30 s, and exclusion duration 90 s.

2.4.4 Data analysis

The *.raw files obtained from the LTQ-OrbiTrap XL were processed by MaxQuant (http://maxquant.org/, version 1.1.1.36) [22] to identify and quantify the phosphopeptides. International Protein Index (IPI) mouse database (v3.52, 55303 entries) was used for database searching and the IPI was converted to RefSeq. Static modification was set as carbamidomethyl on cysteine residues with +57.0215 Da. Variable modifications were set as oxidation on methionine residues with +15.9949 Da; amino termini and lysine residues with +28.0313, +32.0564, and +36.0757 Da, respectively, for light (L), intermediate (M), and heavy (H) isotopic dimethyl labeling and phosphorylation on serine, tryptophan, and tyrosine with +79.9663 Da. Peptides were searched under the conditions of full tryptic cleavage with up to two missed cleavage sites. The other parameters were used as the default setting of the MaxQuant software [22]. Both the protein and peptides identification false-positive rate were less than 5%. The data have been expressed for each individual mass spectral analysis as a $\log_2$ normalized ratio Tg/NonTg. Only the phosphopeptides that had at least two ratios at 2 months and two ratios at 6 months were considered for further analysis. The statistical significances of the phosphopeptide alteration were determined by a two-tailed distribution with two-sample unequal variance Student's *t*-test on the $\log_2$ ratio (Tg/NonTg). The *p*-values were then used to calculate the asymmetric local false-discovery rate (locFDR) [23] by the binomial-based estimator method for each phosphopeptides [24]. A locFDR threshold of 20% (97% of which have a *p*-value less than 0.05) was used as a cut-off to identify phosphopeptides abundance altered over time in Tg mice relative to age-matched NonTg littermates. Molecular functions and protein networks were analyzed by Ingenuity Systems Pathway Analysis software (IPA version 8.8, Ingenuity Systems Inc.).

3 Results

3.1 The reproducibility of the online multidimensional LC-MS/MS system for quantitative phosphoproteome analysis

One challenge in phosphoproteomics is the replicate analysis of the phosphopeptides. In phosphoproteomics, a single phosphopeptide is identified per phosphorylation site in contrast to proteomics, which relies on multiple peptides to identify a protein. This complicates the interpretation of repeat analyses as the same phosphopeptide must be identified in each replicate sample to enable quantification. We recently described a pseudo triplex stable isotope

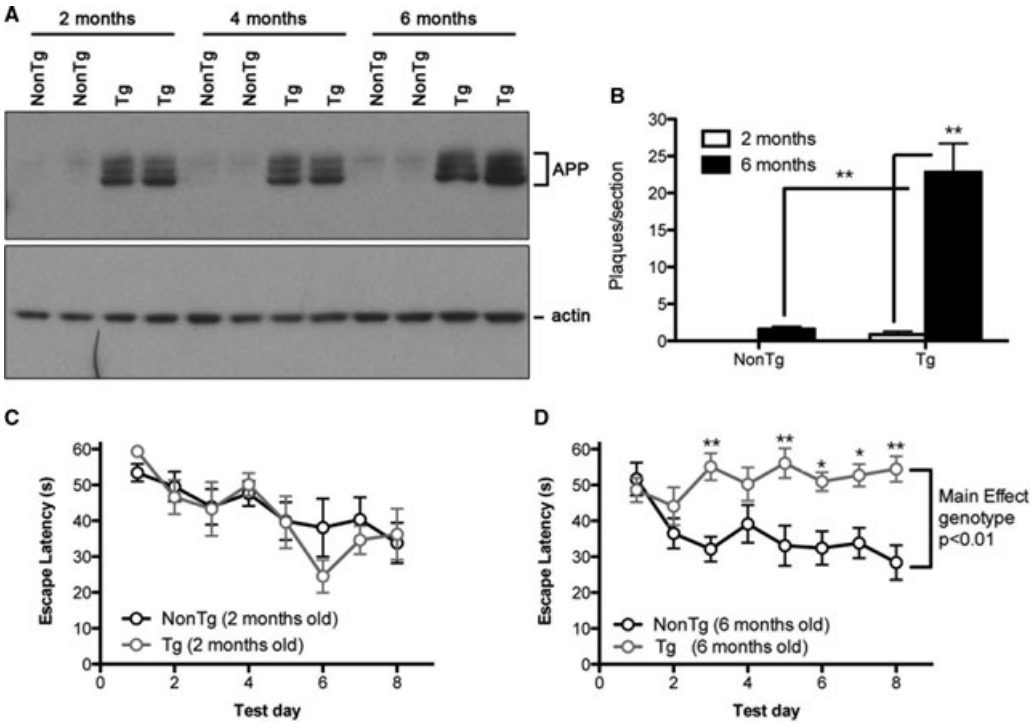

Figure 2. Behavioral impairment in learning and memory is associated with a significant increase in Aβ plaque number and is indicative of conversion from a presymptomatic to a symptomatic state in Tg mice. (A) Western analysis of APP using the 4G8 antibody that detects both murine and human protein. Transgene protein expression is markedly elevated and remains comparable between 2 and 6 months of age in Tg mice. Blots were stripped and reprobed for total myelin basic protein and thus share the same actin loading control (see Fig. 5). (B) Aggregation of 4G8-immunreacive Aβ into compacted and spherical plaque greater than 10 μm in diameter was quantified in $n = 3$ animals per genotype and condition. A significant increase in plaque number was evident at 6 months of age. Statistics were two-way ANOVA as reported in Section 4 followed by Holm–Sidak's tests corrected for multiple comparisons, $^{**}p < 0.01$. (C) Learning and memory as assessed using the Morris Water Maze was comparable between Tg and NonTg mice at 2 months of age. Animals learned to locate the platform and escape the maze at equal rates. (D) Significant impairment in learning and memory was evident by 6 months of age in Tg mice. Statistics were repeated measures (test day) two-way ANOVA (test day and genotype) followed by Holm–Sidak's tests corrected for multiple comparisons to identify significant genotype X test day interactions. $^{*}p < 0.05$, $^{**}p < 0.01$.

dimethyl labeling approach that enables two simultaneous repeat analyses in a single experiment [25]. Here, we applied this approach to phosphopeptide quantification from brain tissue, specifically murine hippocampus. We first tested the performance of the pseudo triplex stable isotope dimethyl labeling for analysis of complex brain samples using protein samples extracted from a NonTg cerebrum to establish reproducibility. Briefly, three 200 μg-tryptic digests of the same protein sample were labeled with L, M, and H isotopic dimethyl groups and mixed together to obtain the standard test sample. Then, the phosphopeptides were enriched and analyzed. The majority of the replicate labeling ratios from identical samples fell between −0.75 and 0.75 ($\log_2$ ratio) with less than 0.1% of the peptides quantified falling outside this limit (Supporting Information Fig. 1). These results indicate that the quantification accuracy of the pseudo triplex stable isotope dimethyl labeling approach is adequate for the study of complex phospho-samples derived from mouse brain.

3.2 Conversion from a presymptomatic to a symptomatic state in the TgCRND8 mouse model is associated with the widespread deposition of Aβ plaques in the hippocampus

Aβ plaque load was established in Tg and NonTg mice at 2 and 6 months of age and behavioral indices of cognition were assessed in the Morris Water Maze at these same time points. Learning and memory impairment in TgCRND8 mice have previously been reported when pathogenic increases in the $A\beta_{42}$ to $A\beta_{40}$ ratio are detected and Aβ oligomers aggregate into plaques within the hippocampus [10]. In mixed hybrid C57BL/6 X C3HF1 TgCRND8 mice, this conversion takes place between 8 and 16 weeks of age with mean age of onset detected at approximately 11 weeks of age [10]. There is, however, considerable variation between animals likely due, in part, to the different genetic backgrounds of different lines [10, 26]. To ensure genetic reproducibility in this study, we backbred C57BL/6 X C3H Tg animals for five generations into a C57BL/6 lineage followed by ten-filial-generation

Figure 3. Cluster analysis of statistically significant changes in relative phosphopeptide abundance $\log_2$(Tg/NonTg) at two (presymptomatic) and 6 (symptomatic) months of age. Increase in phosphorylation is indicated in red, decrease in blue, and not detected in gray. The figure was divided in two parts.

interbreedings. Elevated human APP protein levels in our N5 Tg mice were demonstrated by Western analysis at 2, 4, and 6 months of age. We used the 4G8 antibody to detect both murine and human protein and thereby demonstrate extent of ectopic expression over physiological levels (Fig. 2A). Aβ plaque number was quantitated using the same antibody. Significant increases in Aβ plaque number were detected in 6-month-old Tg animals relative to either age-matched NonTg controls or 2-month-old Tg animals (two-way ANOVA: genotype main effect $F(1,8) = 31.89$; age main effect $F(1,8) = 36.52$; genotype X age interaction $F(1,8) = 27.26$, Fig. 2B). This aggregation corresponded with transition from a presymptomatic to a symptomatic state with respect to behavioral indices of learning and memory in the Morris Water Maze. In this paradigm, mice are required to learn to use minimal external visual cues to find a hidden escape platform submerged in a water pool over an 8 day test period consisting of four training trials per day. At 2 months of age, performance of NonTg and Tg mice was comparable (Fig. 2C). Mice learned to find the escape platform at the same rate exhibiting comparable escape latency over each of the test days. At 6 months of age, a significant main effect of genotype ($F(1,11) = 15.44$ $p < 0.01$ repeated measures two-way ANOVA) and a significant interaction between genotype and test day ($F(7,77) = 2.91$, $p < 0.01$) was detected (Fig. 2D). Tg mice clearly exhibited marked deficiencies in their ability to acquire the task and find the escape platform (Fig. 2C). Swimming velocity was comparable between genotypes indicating impairment of learning and memory and not motoric impairment (data not shown). Taken together, these data demonstrate that N5 C57BL/6 X C3HF10 Tg mice have converted from a presymptomatic phenotype to a symptomatic phenotype by 6 months of age.

3.3 Dynamic changes in the phosphoproteome of TgCRND8 upon conversion from a presymptomatic to a symptomatic state

For phosphoproteomic assessment, two pairs of TgCRND8 and congenic NonTg controls were sacrificed at 2 and 6 months of age. Their hippocampi were carefully excised and the hippocampal proteins were extracted and labeled using the pseudo triplex stable isotope dimethyl labeling approach [25]. Two labeling assignments were performed per analysis. For the first analysis in both 2- and 6-month-old samples, identical amounts (300 μg) of the two NonTg control samples were labeled with L and H dimethyl group, respectively. The Tg comparator mouse sample (300 μg) was labeled with intermediate (M) dimethyl group. Therefore, this procedure enables two replicate quantification comparisons of Tg and NonTg samples in just a single experiment (M/L and M/H). In contrast, for the second biological replicate analysis equal concentrations of the two independent Tg samples (per time point) were labeled with L and H dimethyl group, respectively; and the NonTg mouse control comparator was labeled with intermediate dimethyl group. For each analysis, the three isotopic-labeled samples were mixed and the phosphopeptides were enriched by Ti^{4+}-IMAC followed with nanoflow LC-MS/MS analysis.

We identified 1026 phosphopeptides representing 1168 phosphorylation sites (83% pS, 15% pT, and 2% pY) from 476 unique proteins. Of the 1168 phosphorylations sites, 82% were assigned to a protein kinases according to the PHOSIDA database [27] (Supporting Information Fig. 2), whereas 18% had unknown phosphorylation motifs. Our quantitative analysis using the MaxQuant software [22], to extract intensities for the L, H, and M trios from each replicates and time points, revealed that 595 phosphopeptides from 293 unique proteins could be confidently quantified. Of these, statistically significant changes in the ratios of 139 phosphopeptides were detected in hippocampus of the Tg mice compared to the congenic NonTg control mice upon conversion to a symptomatic state (i.e. 2 versus 6 months of age). Two axis hierarchical clustering, based on the city-block distance with an average linkage analysis, of the significant phosphopeptide changes grouped the results based on age (Fig. 3) whereas clustering performed on the whole phosphoproteomic dataset failed to separate the animal based on age (data not shown). Taken together, these data further identify the subset of phosphosignaling targets altered following symptomatic onset in Tg mice. Bioinformatics analysis of the corresponding protein functions for this phosphopeptide subset revealed that the top five functions are (i) neurological disease, (ii) cellular assembly and organization, (iii) cellular function and maintenance, (iv) cellular movement, and (v) nervous system development and function.

3.4 Network analysis

Protein interaction network analysis for direct protein–protein interactions among the 92 phosphoproteins dynamically regulated in Tg mice between 2 and 6 months of age was performed using Ingenuity Systems Pathway Analysis software. We identified a subset of 36 phosphoproteins that directly interact and whose phosphorylation status is consistently altered upon conversion from a presymptomatic to a symptomatic state (Fig. 4). This protein interaction network points implicates phosphorylation changes in proteins involved in synaptic function and in cytoskeletal maintenance.

4 Discussion

Our phosphoproteome analysis of an early onset mouse model (TgCRND8) of AD reveals specific temporal changes in the phosphoproteome involved in neuronal and glia signaling pathways. We identified 1026 phosphopeptides representing 1168 phosphopeptides of which 595 phosphopeptides were confidently quantified. Of these, 139 phosphopeptides

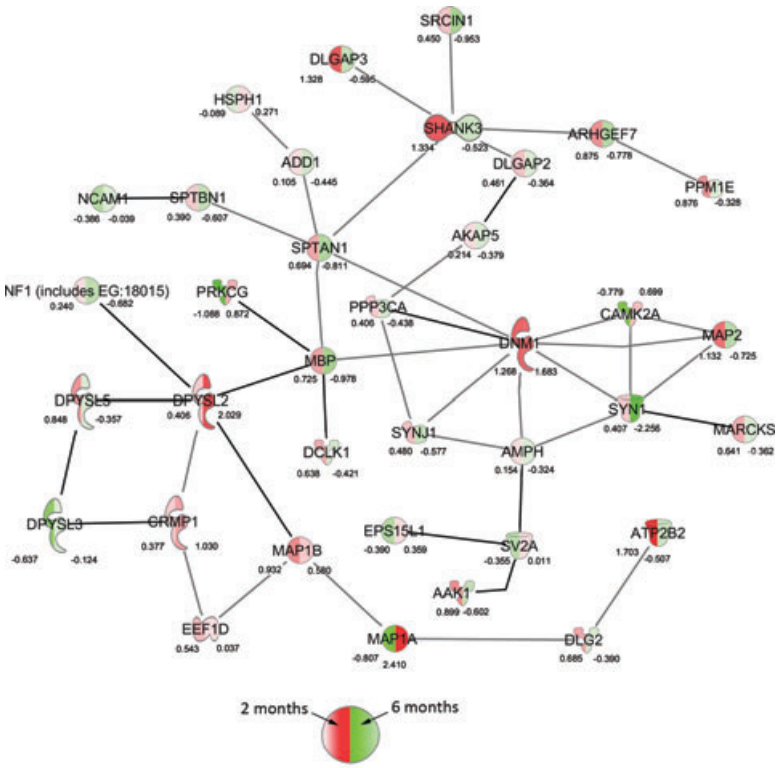

Figure 4. Direct protein–protein interactions between the 92 phosphoproteins whose phosphorylation status changes between 2 and 6 months of age in TgCRND8 mouse model versus congenic littermates. Interaction networks were identified by Ingenuity Pathway Analysis software using curated protein–protein interactions obtained from public databases. Green represents proteins whose average phosphostatus decreases whereas red represents increases in phosphorylation upon conversion from a presymptomatic to symptomatic state.

were found to change in the hippocampus of the Tg mice compared to congenic NonTg control mice over time. This subgroup of phosphopeptides clearly separates the animal according to their symptomatic states (Fig. 3). Moreover, some of these phosphorylated proteins are known to directly interact (Fig. 4).

The clustering analysis and protein interaction network implicates phosphorylation changes in proteins involved in synaptic function and in cytoskeletal maintenance. For example, phosphorylation of the protein SHANK3 (SH3 and multiple ankyrin repeat domains protein 3), which is a large scaffold postsynaptic density protein implicated in dendritic spine and synapse formation, at S856 (TKpSVGEDEKLASLLEGR) was shown to be significantly downregulated 3.6-fold in Tg mice between 2 and 6 months of age but not in NonTg controls over time. A decrease in the level of SHANK3 protein was recently shown to correlate with the progressive accumulation of Aβ oligomers in APP Tg mice [28]. Here, we add to

Table 2. Phosphopeptides observed for the DPYSL protein family

Gene names	Modified sequence	Position	2 months	6 months	Significant
Dpysl1	HAAPAPpSAK	S518	0.4 ± 0.3	−0.88 ± 0.05	a)
Dpysl1	pSSPSKHQPPPIR	S522	0.1 ± 0.2	1.0 ± 0.1	a)
Dpysl1	pSIPHITSDR	S8	0.38 ± 0.04	−0.2 ± 0.1	a)
Dpysl2	TVTPASpSAKpTSPAK	S518, T521	0.5 ± 0.1	−0.4 ± 0.4	
Dpysl2	pTSPAKQQAPPVR	T521	0.0 ± 0.4	2.0 ± 0.1	a)
Dpysl2	TpSPAKQQAPPVR	S522	0.0 ± 0.4	2.0 ± 0.1	a)
Dpysl2	NLHQpSGFSLSGAQIDDNIPR	S537	0.4 ± 0.2	−0.5 ± 0.1	a)
Dpysl2	TVpTPASSAK	T514	0.16 ± 0.09	−0.10 ± 0.06	a)
Dpysl2	NLHQSGFSLpSGAQIDDNIPR	S542	−0.1 ± 0.6	−1.08 ± 0.05	
Dpysl2	TVTPApSSAK	T517	0.1 ± 0.6	0.2 ± 0.2	
Dpysl2	GLYDGPVCEVSVpTPK	T509	0.4 ± 0.1	0.20 ± 0.03	
Dpysl2	pTVTPApSpSAKTSPAK	S517,S518	0.0 ± 0.6	−0.5 ± 0.5	
Dpysl3	GpSPTRPNPPVR	S522	−0.5 ± 0.1	−0.2 ± 0.1	
Dpysl3	GSPpTRPNPPVR	T524	−0.6 ± 0.1	−0.12 ± 0.10	a)
Dpysl5	EMGTPLADpTPTRPVTR	T514	0.85 ± 0.05	−0.36 ± 0.04	a)
Dpysl5	EM(ox)GpTPLADTPTRPVTR	T509	−0.9 ± 0.9	0.14 ± 0.01	

a) Indicates a *p*-value lower than 0.05 and a locFDR lower than 20%.

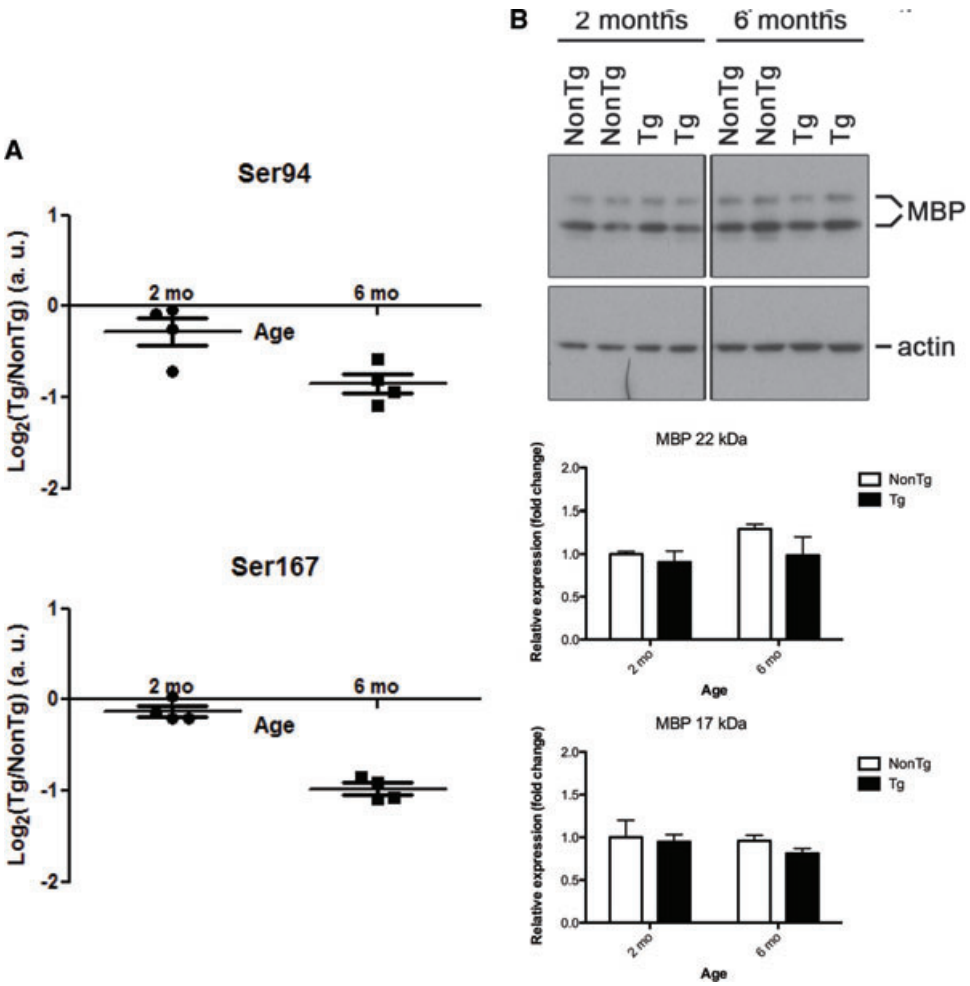

Figure 5. Decreases in phosphorylation of myelin basic protein phosphorylation at S94, and S167 without alteration in total protein levels are detected in symptomatic Tg mice. (A) Statistically significant changes in phosphorylation of MBP and (B) Western blot analysis of two isoforms of MBP. Blots reacted for APP were stripped and reprobed for total myelin basic protein and thus share the same actin loading control (see Fig. 2).

this finding by demonstrating that this decrease is likely also accompanied by a reduction in phosphorylation. Moreover, the SHANK3 complex is important for proper synaptic function and is organized around a Zn^{2+} ion [29]. Aβ is known to affect assembly of the SHANK3 scaffolding platform through the sequestration of Zn^{2+} ions associated with a decrease in hippocampal synapse density [29]. Here, we show that known interactors of SHANK3 such as the protein products of Rho guanine nucleotide exchange factor (GEF) 7 (ARHGEF7), and discs, large homolog-associated protein such as DLGAP2 and DLGAP3 show similar regulation trends in phosphoregulation. Thus, a known signaling network implicated in AD synaptic dysfunction is disrupted not only at the transcriptional/translation level [29] but also at the post-translational level. Clearly, it will be essential to explore the functional significance of SHANK3 phosphorylation and its decrease during the transition from a presymptomatic to a symptomatic disease state in AD.

Our unbiased phosphoproteome analysis also reveals differential regulation of many proteins involved in cytoskeletal functions in symptomatic Tg mice. In particular, the dihydropyrimidinase-related proteins DPYSL1–5 (also named CRMP1–5) are known to form homo-/hetero tetramers and to mediate Semaphorin3A and neurotrophin signaling leading to cytoskeletal rearrangement [30]. Although their phosphorylation has been previously reported, the change in levels of phosphorylation found here during the symptomatic progression in a mouse model of Aβ deposition is novel (Table 2). Interestingly, it was recently demonstrated that the phosphorylation of DPYSL1 and DPYSL2 at a position S522 by the cyclin-dependent kinase 5 (CDK5) are involved in axonal guidance and spine development and that the loss of S522 phosphorylation leads to abnormal dendritic patterning [31]. Phosphorylation at S522 in DPYSL2 has been shown to decrease its binding affinity to tubulin and Numb, as well as facilitate its phosphorylation by glycogen synthase kinase-3 beta (GSK3β) [32–34]. DPYSL2 is hyperphosphorylated in human brain and some animal models of AD at both GSK3β (T514) and CDK5 (S522) consensus sites [35]. However, the phosphorylation of DPYSL3 at T509, by GSK3β has not been found to increase in human AD at postmortem analysis [35]. Here, we also observed an increase in the ratio (Tg/NonTg) of CDK5-dependent phosphorylation of DPYSL1 (twofold) and DPYSL2 (fourfold) but not

Table 3. Phosphopeptides observed for the tau protein

Modified sequence	Position in the mouse canonical sequence (NP001033698.1/ 733 aa)	Position in the human canonical sequence (NP058519.3/ 758 aa)	Position in the human consensus sequence in the field (NP005901.2/441aa)	2 months	6 months	Significant
SGYSpSPGSPGTPGSR	Ser491	Ser516	Ser199	−0.2 ± 0.1	0.5 ± 0.1	
SGYSSPGpSPGTPGSR	Ser494	Ser519	Ser202	0.0 ± 0.1	0.4 ± 0.1	
TPpSLPTPPTREPK	Ser506	Ser531	Ser214	0.3 ± 0.1	0.4 ± 0.1	
TPPKpSPSASK	Ser527	Ser552	Ser235	1.1 ± 0.1	−0.7 ± 0.1	a)
TPPKSPpSASK	Ser529	Ser554	Ser237	0.4 ± 0.1	−0.3 ± 0.2	
TDHGAEIVYKpSPVVSGDpTSP	Ser688/Thr695	Ser713/Thr720	Ser396/Thr403	0.2 ± 0.1	−0.1 ± 0.1	
SPVVpSGDTSPR	Ser692	Ser717	Ser400	−0.4 ± 0.1	0.8 ± 0.1	a)
SPVVSGDTpSPR	Ser696	Ser721	Ser404	0.0 ± 0.1	0.3 ± 0.1	
TTPSPKpTPPGSGEPPK	Thr473	Thr498	Thr181	−0.1 ± 0.1	1.1 ± 0.1	a)
VAVVRpTPPKSPSASK	Thr523	Thr548	Thr231	−0.1 ± 0.1	0.1 ± 0.1	
SPVVSGDpTSPR	Thr695	Thr720	Thr403	−0.1 ± 0.1	0.3 ± 0.1	
GAApSPAQK	Ser451	—	—	1.5 ± 0.7	0.1 ± 0.3	
TTPpSPKTPPGSGEPPKSGER	Ser470	—	—	−0.1 ± 0.1	0.8 ± 0.2	

a) Indicates a *p*-value lower than 0.05 and a locFDR lower than 20%.

DPYSL3 (not significant) at a position S522 upon conversion from presymptomatic to symptomatic stage. Our observed changes in phosphorylation at S522 are in agreement with what has been previously observed in human postmortem tissues [35]. In contrast, the changes in phosphorylation that are dependent on GSK3β on DPYSL1 (S518, twofold decrease), DPYSL5 (T514, twofold decrease), and DPYSL2 and 5 (T509, no changes) were not detected or, surprisingly, changed in the opposite direction compared to what has been previously reported in human. Further, we observed an increase in phosphorylation at T524 (increase) of DPYSL3 in symptomatic Tg mice. The phosphorylation of DPYSL3 at T524 has been previously postulated based on MALDI data [36]. Finally, we report a statistically significant decrease in a new phosphorylation site at position S8 of the N-terminal of DPYSL1 in Tg compared to NonTg mice at both 2 and 6 months of age. Taken together, these data suggest that, in the TgCRND8 AD mouse model, changes in CDK5-dependent phosphorylation of DPSYL proteins recapitulate those detected in postmortem human tissue whereas the GSK3β-dependent events are not consistently reproduced. It is tempting to speculate that this disconnect between mouse and human data may, in part, contribute to the lack of cytoskeletal rearrangement in the TgCRND8 mouse model upon conversion to a symptomatic state and it would be interesting to establish whether older animals, representative of late-stage AD, would eventually exhibit this stepwise progression in dysfunctional phosphosignaling.

A similar intermediate pattern was detected with respect to phosphorylation and interaction between DPYSL2 and MAP1b [37]. Both DPYSL1 and DPYSL2 have been shown to interact with MAP1b in a GSK3β-dependent manner [38]. Interestingly, both DPYSL proteins and MAP1b are part of the semaphorin 3A signaling network and are phosphorylated by both CDK5 and GSK-3β. We observed numerous phosphorylated peptides on MAP1b; however, only one was altered over time in Tg mice compared to NonTg controls (TIKpTPEDGGYTCEITEK) with over a twofold decrease (CK2 site). A fivefold increase in the relative abundance of phosphorylated microtubule-associated protein 1A (MAP1a) (EpTSPTRGEPVPAWEGK; predicted PKA site) and a twofold increase in both the GSK3β (ARVDHGAEIITQpSPSR) and CK1 sites (VDHGAEIITQSPpSR) on microtubule-associated protein 2 (MAP2) were also detected upon symptomatic conversion in Tg mice. Again, the majority of GSK3β phosphorylation sites on MAP1a, microtubule-associated protein 1B (MAP1b), and MAP2 detected in both Tg and NonTg mice at 2 and 6 months of age did not change in this study which may, in part, also underlie why neuronal cytoskeletal integrity is not compromised in TgCRND8 mice exhibiting both significant Aβ plaque load and behavioral indices of learning and memory.

Changes in glia phospho-networks were also detected. A decrease in the abundance of MBP phosphorylated on two different sites was found without a change in on total MBP levels (Fig. 5). One of the primary functions of MBP is to participate in the adhesion of myelin by binding negatively charged lipids at the membrane on the cytosolic membrane leaflet of oligodendrocytes [39]. In this configuration, MBP can also act as scaffold for other molecules including SH3-containing proteins [40] and actin [41]. Interestingly, phosphorylation of MBP reduces its ability to attach actin to membrane microdomains enriched in negatively charged lipids as would be predicted in lipid rafts [41]. Thus, the decrease in MBP phosphorylation in symptomatic Tg mice may be indicative of a compensatory attempt to increase MBP scaffolding of actin and other molecules to the negatively charged lipids at the membrane, potentially within raft domains.

Finally, differences and similarities in post-translational murine tau modification were detected following symptomatic conversion in TgCRND8 mice compared to clinical AD. Hyperphosphorylated tau, aggregating into fibrils, protofibrils, and finally intraneuronal neurofibrillary tangles is a hallmark pathology of AD. In this study, we quantified 13 phosphopeptides (Table 3) in murine tau. To assess relevancy to clinical AD, we aligned these phospho-amino acid sequences to that of the 441 amino acid isoform of human tau (NP_005901.2). Two phosphopeptides represented sites not conserved in the human sequence: GAApSPAQK and TTPpSPKTPPGSGEPPKSGER. Ten tau phosphopeptides were found to be singly phosphorylated and one was shown to be doubly phosphorylated (S396 and T403). Of these, a twofold increase in the abundance of tau phosphopeptides phosphorylated at T181 and S400, and a 3.4-fold decrease in abundance of phosphopeptides phosphorylated at S235 were detected upon conversion to a symptomatic state in Tg mice compared to NonTg control. Human tau fibrillization is precipitated by phosphorylation at T231, S262, T181, S199, S202, T212, S396, T403, and S404 [42]. We did not detect T212 and S262 phosphoresidues in Tg mice. Moreover, the abundance of protein phosphorylation at S199, S202, T231, T403, and S404 and the doubly phosphorylated S396 and T403 phosphorylation were not altered by age or genotype. Only T181 showed an incrased phosphorylation in the TgCRND8 mouse model exhibiting impairment in behavioral indices of learning and memory. CDK5 has been shown to phosphorylate tau at S202, S235, and S404 [43]. Phosphorylation by CDK5 at S235 primes tau for phosphorylation by GSK3β at T231; phosphorylation by CDK5 at S404 primes tau for sequential phosphorylation by GSK3β at S396 and S400 [44]. Surprisingly, we found that, in symptomatic TgCRND8 mice, phosphorylation at S235 was reduced between 2 and 6 months suggesting that CDK5 is not priming tau for phosphorylation by GSK3β at T231 (wherein no change in phosphorylation was detected in this study). In contrast, GSK3β-dependent phosphorylation of tau at S400 (but not S396) was observed to increase between 2 and 6 months without a concomitant phospho-priming by CDK5 at S404. These data highlight a primary difference between the TgCNRD8 mouse model of AD and the human condition. Moreover, hyperphosphorylation at T181, S202, and T231 has been shown to occur early in the formation of neurofibrillary tangles whereas hyperphosphorylation at S396 and S404 occur later in the aggregation process [45]. Here, only phosphorylation at T181 of tau increased upon conversion to a symptomatic state. These differences hint at underlying mechanisms through which tau hyperphosphorylation but not aggregate assembly into neurofibrillary tangles is observed in the TgCRND8 mice [10, 46].

In summary, our study of the hippocampal phosphoproteome in presymptomatic and symptomatic TgCRND8 mice, normalized-to-age-dependent changes in control animals, identifies network-wide changes in protein phosphorylation associated with Aβ accumulation, extracellular deposition, and learning and memory impairment. Targets include phospho-dependent pathways linked to AD as well as differences between murine and human conversion to a symptomatic state that may underlie differences between murine models of Aβ deposition and the human AD condition.

H. Z. acknowledges the Creative Research Group Project from NSFC (Grant No. 21021004) and the China–Canada Joint Health Research Initiative from NSFC (Grant No. 81161120540). D. F. acknowledges a Canada Research Chair in Proteomics and Systems Biology. D. F. and S. B. acknowledge funding from CIHR (CCI-117960 and TGF-96121). F. W., A. P. B., and M. G. received studentship support from the CIHR Training Program in Neurodegenerative Lipidomics (TGF-96121). A. P. B. is further supported by a doctoral fellowship from FRSQ. H. X. received a MITACs fellowship. We thank Mark Akins for his technical expertise and assistance in backcrossing the TgCRND8 line into a C57BL/6 background.

The authors have declared no conflict of interest.

5 References

[1] Goedert, M., Spillantini, M. G., A century of Alzheimer's disease. *Science* 2006, *314*, 777–781.

[2] Cleary, J. P., Walsh, D. M., Hofmeister, J. J., Shankar, G. M. et al., Natural oligomers of the amyloid-beta protein specifically disrupt cognitive function. *Nat. Neurosci.* 2005, *8*, 79–84.

[3] Bernstein, S. L., Wyttenbach, T., Baumketner, A., Shea, J. E. et al., Amyloid beta-protein: monomer structure and early aggregation states of Abeta42 and its Pro19 alloform. *J. Am. Chem. Soc.* 2005, *127*, 2075–2084.

[4] Selkoe, D. J., Alzheimer's disease is a synaptic failure. *Science* 2002, *298*, 789–791.

[5] Nimmrich, V., Ebert, U., Is Alzheimer's disease a result of presynaptic failure? Synaptic dysfunctions induced by oligomeric beta-amyloid. *Rev. Neurosci.* 2009, *20*, 1–12.

[6] Herrup, K., Reimagining Alzheimer's disease–an age-based hypothesis. *J. Neurosci.* 2010, *30*, 16755–16762.

[7] Reddy, P. H., Abnormal tau, mitochondrial dysfunction, impaired axonal transport of mitochondria, and synaptic deprivation in Alzheimer's disease. *Brain Res.* 2011, *1415*, 136–148.

[8] Bierer, L. M., Hof, P. R., Purohit, D. P., Carlin, L. et al., Neocortical neurofibrillary tangles correlate with dementia severity in Alzheimer's disease. *Arch. Neurol.* 1995, *52*, 81–88.

[9] Di Domenico, F., Sultana, R., Barone, E., Perluigi, M. et al., Quantitative proteomics analysis of phosphorylated proteins in the hippocampus of Alzheimer's disease subjects. *J. Proteomics* 2011, *74*, 1091–1103.

[10] Chishti, M. A., Yang, D. S., Janus, C., Phinney, A. L. et al., Early-onset amyloid deposition and cognitive deficits in transgenic mice expressing a double mutant form of amyloid precursor protein 695. *J. Biol. Chem.* 2001, *276*, 21562–21570.

[11] Van Vickle, G. D., Esh, C. L., Kalback, W. M., Patton, R. L. et al., TgCRND8 amyloid precursor protein transgenic mice exhibit an altered gamma-secretase processing and an aggressive, additive amyloid pathology subject to immunotherapeutic modulation. *Biochemistry* 2007, *46*, 10317–10327.

[12] Janus, C., Pearson, J., McLaurin, J., Mathews, P. M. et al., A beta peptide immunization reduces behavioural impairment and plaques in a model of Alzheimer's disease. *Nature* 2000, *408*, 979–982.

[13] Phinney, A. L., Drisaldi, B., Schmidt, S. D., Lugowski, S. et al., In vivo reduction of amyloid-beta by a mutant copper transporter. *Proc. Natl. Acad. Sci. USA* 2003, *100*, 14193–14198.

[14] Wong, G. T., Manfra, D., Poulet, F. M., Zhang, Q. et al., Chronic treatment with the gamma-secretase inhibitor LY-411,575 inhibits beta-amyloid peptide production and alters lymphopoiesis and intestinal cell differentiation. *J. Biol. Chem.* 2004, *279*, 12876–12882.

[15] Supnet, C., Grant, J., Kong, H., Westaway, D., Mayne, M., Amyloid-beta-(1–42) increases ryanodine receptor-3 expression and function in neurons of TgCRND8 mice. *J. Biol. Chem.* 2006, *281*, 38440–38447.

[16] McLaurin, J., Kierstead, M. E., Brown, M. E., Hawkes, C. A. et al., Cyclohexanehexol inhibitors of Aβ aggregation prevent and reverse Alzheimer phenotype in a mouse model. *Nat. Med.* 2006, *12*, 801–808.

[17] Wessel, D., Flugge, U. I., A method for the quantitative recovery of protein in dilute solution in the presence of detergents and lipids. *Anal. Biochem.* 1984, *138*, 141–143.

[18] Boersema, P. J., Raijmakers, R., Lemeer, S., Mohammed, S., Heck, A. J., Multiplex peptide stable isotope dimethyl labeling for quantitative proteomics. *Nat. Protoc.* 2009, *4*, 484–494.

[19] Yu, Z., Han, G., Sun, S., Jiang, X. et al., Preparation of monodisperse immobilized Ti(4+) affinity chromatography microspheres for specific enrichment of phosphopeptides. *Anal. Chim. Acta* 2009, *636*, 34–41.

[20] Wang, F., Dong, J., Jiang, X., Ye, M., Zou, H., Capillary trap column with strong cation-exchange monolith for automated shotgun proteome analysis. *Anal. Chem.* 2007, *79*, 6599–6606.

[21] Wang, F., Chen, R., Zhu, J., Sun, D. et al., A fully automated system with online sample loading, isotope dimethyl labeling and multidimensional separation for high-throughput quantitative proteome analysis. *Anal. Chem.* 2010, *82*, 3007–3015.

[22] Cox, J., Mann, M., MaxQuant enables high peptide identification rates, individualized p.p.b.-range mass accuracies and proteome-wide protein quantification. *Nat. Biotechnol.* 2008, *26*, 1367–1372.

[23] Bickel, D. R., Simple estimators of false discovery rates given as few as one or two p-values without strong parametric assumptions. *ArXiv e-prints* 2011, 2011arXiv1106.4490B.

[24] Hong, W. J., Tibshirani, R., Chu, G., Local false discovery rate facilitates comparison of different microarray experiments. *Nucleic Acids Res.* 2009, *37*, 7483–7497.

[25] Song, C., Wang, F., Ye, M., Cheng, K. et al., Improvement of the quantification accuracy and throughput for phosphoproteome analysis by a pseudo triplex stable isotope dimethyl labeling approach. *Anal. Chem.* 2011, *83*, 7755–7762.

[26] Glazner, K. A., Odero, G. L., Anema, E., Motnenko, A. et al., Strain specific differences in memory and neuropathology in a mouse model of Alzheimer's disease. *Life Sci.* 2010, *86*, 942–950.

[27] Gnad, F., Gunawardena, J., Mann, M., PHOSIDA 2011: the posttranslational modification database. *Nucleic Acids Res.* 2011, *39*, D253–D260.

[28] Verpelli, C., Dvoretskova, E., Vicidomini, C., Rossi, F. et al., Importance of Shank3 protein in regulating metabotropic glutamate receptor 5 (mGluR5) expression and signaling at synapses. *J. Biol. Chem.* 2011, *286*, 34839–34850.

[29] Grabrucker, A. M., Schmeisser, M. J., Udvardi, P. T., Arons, M. et al., Amyloid beta protein-induced zinc sequestration leads to synaptic loss via dysregulation of the ProSAP2/Shank3 scaffold. *Mol. Neurodegener.* 2011, *6*, 65.

[30] Yamashita, N., Goshima, Y., Collapsin response mediator proteins regulate neuronal development and plasticity by switching their phosphorylation status. *Mol. Neurobiol.* 2012, *45*, 234–246.

[31] Yamashita, N., Ohshima, T., Nakamura, F., Kolattukudy, P. et al., Phosphorylation of CRMP2 (collapsin response mediator protein 2) is involved in proper dendritic field organization. *J. Neurosci.* 2012, *32*, 1360–1365.

[32] Uchida, Y., Ohshima, T., Sasaki, Y., Suzuki, H. et al., Semaphorin3A signalling is mediated via sequential Cdk5 and GSK3beta phosphorylation of CRMP2: implication of common phosphorylating mechanism underlying axon guidance and Alzheimer's disease. *Genes Cells* 2005, *10*, 165–179.

[33] Cole, A. R., Causeret, F., Yadirgi, G., Hastie, C. J. et al., Distinct priming kinases contribute to differential regulation of collapsin response mediator proteins by glycogen synthase kinase-3 in vivo. *J. Biol. Chem.* 2006, *281*, 16591–16598.

[34] Nishimura, T., Fukata, Y., Kato, K., Yamaguchi, T. et al., CRMP-2 regulates polarized Numb-mediated endocytosis for axon growth. *Nat. Cell Biol.* 2003, *5*, 819–826.

[35] Cole, A. R., Noble, W., van Aalten, L., Plattner, F. et al., Collapsin response mediator protein-2 hyperphosphorylation is an early event in Alzheimer's disease progression. *J. Neurochem.* 2007, *103*, 1132–1144.

[36] Zhou, Y., Bhatia, I., Cai, Z., He, Q. Y. et al., Proteomic analysis of neonatal mouse brain: evidence for hypoxia- and ischemia-induced dephosphorylation of collapsin response mediator proteins. *J. Proteome Res.* 2008, *7*, 2507–2515.

[37] Good, P. F., Alapat, D., Hsu, A., Chu, C. et al., A role for semaphorin 3A signaling in the degeneration of hippocampal neurons during Alzheimer's disease. *J. Neurochem.* 2004, *91*, 716–736.

[38] Lin, P. C., Chan, P. M., Hall, C., Manser, E., Collapsin response mediator proteins (CRMPs) are a new class of microtubule-associated protein (MAP) that selectively interacts with assembled microtubules via a taxol-sensitive binding interaction. *J. Biol. Chem.* 2011, *286*, 41466–41478.

[39] Boggs, J. M., Rangaraj, G., Gao, W., Heng, Y. M., Effect of phosphorylation of myelin basic protein by MAPK on its interactions with actin and actin binding to a lipid membrane in vitro. *Biochemistry* 2006, *45*, 391–401.

[40] Polverini, E., Rangaraj, G., Libich, D. S., Boggs, J. M., Harauz, G., Binding of the proline-rich segment of myelin basic protein to SH3 domains: spectroscopic, microarray, and modeling studies of ligand conformation and effects of post-translational modifications. *Biochemistry* 2008, *47*, 267–282.

[41] Boggs, J. M., Rangaraj, G., Heng, Y. M., Liu, Y., Harauz, G., Myelin basic protein binds microtubules to a membrane surface and to actin filaments in vitro: effect of phosphorylation and deimination. *Biochim. Biophys. Acta 2011, 1808*, 761–773.

[42] Wang, J. Z., Grundke-Iqbal, I., Iqbal, K., Kinases and phosphatases and tau sites involved in Alzheimer neurofibrillary degeneration. *Eur. J. Neurosci.* 2007, *25*, 59–68.

[43] Illenberger, S., Zheng-Fischhofer, Q., Preuss, U., Stamer, K. et al., The endogenous and cell cycle-dependent phosphorylation of tau protein in living cells: implications for Alzheimer's disease. *Mol. Biol. Cell* 1998, *9*, 1495–1512.

[44] Li, T., Hawkes, C., Qureshi, H. Y., Kar, S., Paudel, H. K., Cyclin-dependent protein kinase 5 primes microtubule-associated protein tau site-specifically for glycogen synthase kinase 3beta. *Biochemistry* 2006, *45*, 3134–3145.

[45] Noble, W., Olm, V., Takata, K., Casey, E. et al., Cdk5 is a key factor in tau aggregation and tangle formation in vivo. *Neuron* 2003, *38*, 555–565.

[46] Ryan, S. D., Whitehead, S. N., Swayne, L. A., Moffat, T. C. et al., Amyloid-beta42 signals tau hyperphosphorylation and compromises neuronal viability by disrupting alkylacylglycerophosphocholine metabolism. *Proc. Natl. Acad. Sci. USA* 2009, *106*, 20936–20941.

